Preprint
UCRL-JC-146627

Mapping Phase Transformations in the Heat-Affected-Zone of Carbon Manganese Steel Welds using Spatially Resolved X-Ray Diffraction

J. W. Elmer, J. Wong, T. Ressler, T. A. Palmer

This article was submitted to
6th International Conference on Trends in Welding Research, Pine Mountain, GA., April 15-19, 2002

U.S. Department of Energy

Lawrence Livermore National Laboratory

December 4, 2001

This work was performed under the auspices of the United States Department of Energy by the University of California, Lawrence Livermore National Laboratory under contract No. W-7405-Eng-48.

Mapping Phase Transformations in the Heat-Affected-Zone of Carbon Manganese Steel Welds using Spatially Resolved X-Ray Diffraction

John W. Elmer, Joe Wong, Thorsten Ressler and Todd A. Palmer

Abstract

Spatially Resolved X-Ray Diffraction (SRXRD) was used to investigate phase transformations that occur in the heat affected zone (HAZ) of gas tungsten arc (GTA) welds in AISI 1005 carbon-manganese steel. *In situ* SRXRD experiments performed at the Stanford Synchrotron Radiation Laboratory (SSRL) probed the phases present in the HAZ during welding, and these real-time observations of the HAZ phases were used to construct a map of the phase transformations occurring in the HAZ. This map identified 5 principal phase regions between the liquid weld pool and the unaffected base metal for the carbon-manganese steel studied in this investigation. Regions of annealing, recrystallization, partial transformation and complete transformation to α-Fe, γ-Fe, and δ-Fe phases were identified using SRXRD, and the experimental results were combined with a heat flow model of the weld to investigate transformation kinetics under both positive and negative temperature gradients in the HAZ. From the resulting phase transformation map, the kinetics of phase transformations that occur under the highly non-isothermal heating and cooling cycles produced during welding of steels can now be better understood and modeled.

Introduction

Microstructural gradients are created in the HAZ of fusion welds by solid-state transformations such as grain growth, recrystallization, phase changes, annealing, and tempering [1-4]. In steel, these transformations result in the formation of different microstructural sub-regions that are referred to as the coarse grained region, the fine grained region, and the partially transformed region of the HAZ [1-4]. The presence of these different HAZ regions is known in a qualitative sense, however, their exact size and location is not well understood because they depend on both the heating cycle of the weld and the kinetics of the phase transformations. Although the heating cycle of the weld can be modeled and/or experimentally measured, the kinetics of each of the various phase transformations are difficult to determine and are rarely known under actual welding conditions. This lack of information has hindered both the during cooling of the HAZ [2]. However, the prediction of weld microstructures from CCT diagrams requires many assumptions in order to deal with the non-isothermal and non-uniform cooling conditions of welds [2], particularly under the high temperature gradients produced by intense laser beam welding [5,6]. Furthermore, these diagrams represent the *cooling* but not the *heating* portions of the HAZ, and there is no generally accepted method for verifying how well these diagrams predict actual HAZ behavior.

Modeling the phase transformations that occur in the HAZ during welding requires both a good understanding of the temperature cycles that occur during welding and kinetics of the phase transformations. Numerical modeling of the weld temperatures has advanced considerably in the past few years and is now being used by weld researchers to calculate the size and shape of the fusion zone in carbon stels [7-9] and other alloys such as titanium [10]. These models provide accurate information about transient three-dimensional temperature distribution around the weld, allowing the spatial distribution of peak temperatures, heating rates and cooling rates in the HAZ to be determined. However, without corresponding phase transformation kinetic models, microstructural evolution in the weld HAZ cannot be predicted. In this investigation we present SRXRD as a novel and unique experimental method for investigating microstructural evolution by directly mapping the phases that exist in the HAZ *during* welding.

Materials and Experimental Procedures

AISI 1005 steel in the form of 10.8 cm diameter forged bar stock was used for all of the experiments. Chemical analysis was performed on this material using combustion analysis for O, C, N, and H, and inductively coupled plasma analysis for the remaining elements. The results yield the following concentration (by wt. percent): 0.05 C, 0.31 Mn, 0.18 Si, 0.11 Ni, 0.10 Cr, 0.009 P, 0.008 Cu, 0.005 S, <0.005 Al, <0.005 Nb, <0.005 Mo, <0.005 Ti, <0.005 V. Cylindrical welding samples were machined from the as received steel into 10.2 cm diameter bars measuring 12.7 cm long

Gas tungsten arc welds were made on the steel bars using a 225 A direct constant current welding power supply with electrode negative polarity. The average power was maintained constant at 1.9 kW (110 A, 17.5 V) for all of the welds. Helium was used as the welding and shielding gas, and the welds were made with the torch inclined 30° from being perpendicular to the surface of the bar to prevent blocking of the diffracted x-rays. The steel bar was rotated below the fixed electrode at a constant speed of 0.11 rpm, which corresponded to a surface welding speed of 0.6 mm/s, and resulted in a ~9 mm wide fusion zone on the surface of the steel bar.

The SRXRD measurements were performed during welding using the 31-pole wiggler beam line, BL 10-2 [11] at SSRL with SPEAR (Stanford Positron-Electron Accumulation Ring) operating at an electron energy of 3.0 GeV and an injection current of ~100 mA. Details of the SRXRD welding experiments have been previously published [12-15] so only a brief description will be given here to point out some modifications to the technique.

A typical SRXRD run consisted of gathering 40 diffraction patterns, each spaced 250 μm apart, along a pre-determined path to span a range of 10 mm through the HAZ. A software package was developed on a personal computer using LabView software to control the position of the weld with respect to the x-ray beam, to control the bar rotational speed (welding speed), and to trigger the data acquisition system on a second computer. Each SRXRD data point was taken while the beam was at a fixed location with respect to the welding electrode, and data was collected for 10 s while the bar rotated under the torch at a constant speed. The resulting data was presented as a series of x-ray diffraction patterns along a given x-ray scan direction perpendicular to and away from the centerline of the weld. After completing a run, the weld was allowed to cool to room temperature and the weld was repositioned to a new starting location with respect to the x-ray beam prior to taking the next series of SRXRD data.

Results and Discussion

Phase Equilibria. Pure iron exists in both the body centered cubic (bcc) and face centered cubic (fcc) crystal forms [16]: α-Fe and δ-Fe are both bcc, while γ-Fe is fcc. In pure iron, α-Fe transforms to γ-Fe at 910°C, which is referred to as the A3 temperature. The γ-Fe reverts back to the bcc phase (now called δ-Fe) at 1390°C, which is referred to as the A4 temperature. The δ-Fe then remains stable up to the melting point at 1536°C. The AISI 1005 carbon manganese steel used in this investigation is similar in that it goes through each of these phase transformations but the microstructure also contains carbides at lower temperatures [16]. These carbides, for example cementite, transform to a mixture of α-Fe (ferrite) and γ-Fe (austenite) at 727°C, which is called the A1 temperature in Fe-C alloys. The principal phase transformation temperatures are commonly referred to as the A_C1, A_C3 and A_C4 on heating, and the A_R1, A_R3 and A_R4 on cooling.

Manganese, silicon and trace impurities present in the 1005 steel further alter the phase transformation temperatures, and these changes can be calculated from thermodynamic relationships. Thermocalc [17] was used to calculate the phase transformation temperatures for the particular AISI 1005 steel used in this investigation by S. S. Babu [18]. These calculations were made by considering the effects of Fe, C, Si, Mn, Ni and Cr on the liquid, ferrite, austenite, and cementite phase fields. The results of the phase-boundary temperatures, as calculated by Thermocalc for this multi-component alloy, are summarized in Table 1 and are illustrated in pseudo-binary form in Fig. 1. The first transformation on heating begins at 720°C as the carbides dissolve, leaving a mixture of α-Fe and γ-Fe. The α-Fe disappears at 882°C, leaving γ-Fe as the only solid phase up to 1432°C when δ-Fe first appears. The δ-Fe coexists with γ-Fe up to 1462°C where γ-Fe disappears, leaving δ-Fe as the only solid phase up to the melting point at 1529°C.

Table 1 Calculated phase transformation temperatures for the AISI 1005 carbon manganese steel.

Transformation events On heating	Transformation	Temperature (°C)
cementite disappears (Ac1)	$Fe_3C \rightarrow (\alpha+\gamma)$	720
α–ferrite disappears (Ac3)	$(\alpha+\gamma) \rightarrow \gamma$	882
δ–ferrite reappears (Ac4)	$\gamma \rightarrow (\gamma+\delta)$	1432
austenite disappears	$(\gamma+\delta) \rightarrow \delta$	1462
liquid appears	$\delta \rightarrow (\delta+L)$	1506
ferrite disappears (liquidus)	$(\delta+L) \rightarrow L$	1529

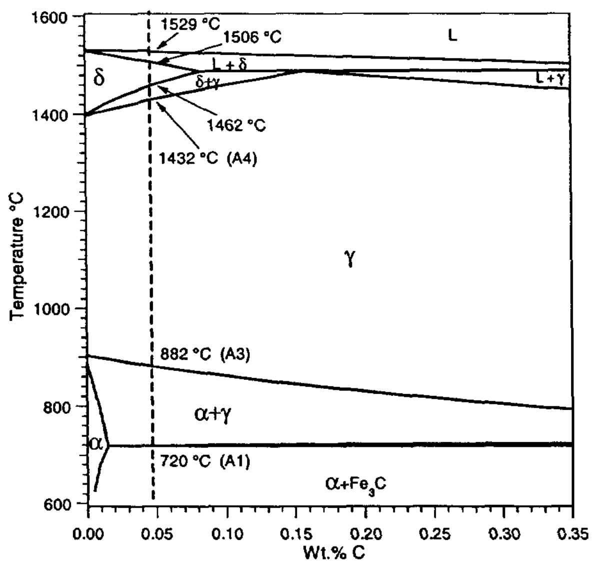

Figure 1 : Calculated pseudobinary Fe-C phase diagram for the AISI 1005 steel [18].

Base Metal and HAZ Microstructures. The microstructure of the HAZ was revealed by lightly polishing the surface of the welded steel bar and then etching in a 2% nital (nitric acid and alcohol) solution. Figure 2a shows the base metal microstructure, which is largely composed of equiaxed ferrite grains having an average diameter of 21.6 μm. Small regions of pearlite are present in the base metal microstructure at grain boundary edges and corners.

As welding proceeds, these new γ-Fe grains in the fine-grained region of the HAZ grow. The amount of grain growth increases rapidly as the weld fusion zone is approached, leading to the formation of the coarse grained microstructural region of the HAZ. This coarse grained region of the HAZ is adjacent to the weld fusion zone and contains grains larger than those in the base metal. The coarse grained region is shown in Fig. 2b at a location 0.25 mm from the fusion line. This microstructure contains primarily α-Fe grains (at room temperature) that have transformed from the large prior γ-Fe grains.

The width of each microstructural subregion was measured on the metallographically prepared samples, showing that the coarse grained microstructural region extended 0.75 mm from the fusion line, the fine grained region extended an additional 1.25 mm from the edge of the coarse grained region, and the partially transformed region extended an additional 1.0 mm from the edge of the fine grained region. The total width of the HAZ is equal to the sum of the widths of the three subregions, which measured 3.0 mm. Using the SRXRD technique, we can now follow in detail the evolution of the HAZ and various microstructural subregions contained therein as the base metal is heated and transforms along various thermal gradients during the welding process.

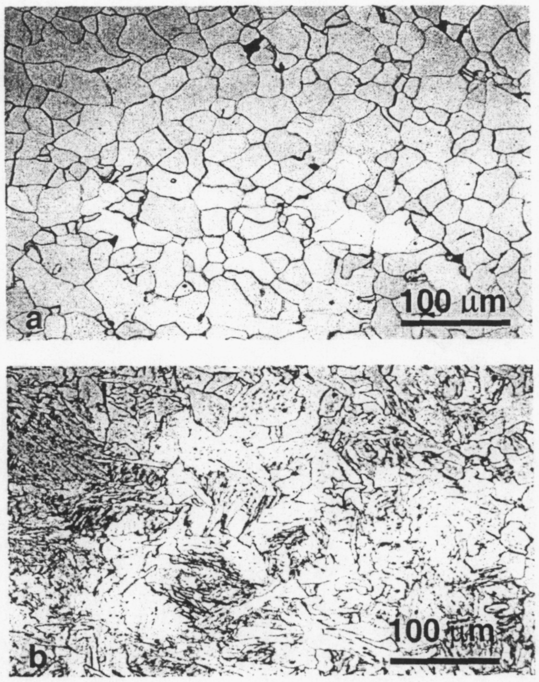

Figure 2: Optical micrographs of AISI 1005 steel fusion weld for (a) base metal, and (b) coarse grained region of the HAZ.

SRXRD Patterns. SRXRD experiments were performed *in-situ,* allowing the spatial distribution of phases present in the HAZ during welding to be dedtermined. Diffraction patterns from the α-Fe, γ-Fe, and δ-Fe phases at specific locations within the HAZ were collected during welding. For the 1005 steel, the Bragg peaks for each of the phases were calculated [19] using the lattice constants of pure iron at room temperature: 0.28665nm for the bcc phase and 0.3666nm for the fcc phase [20]. Figure 3 shows the results of these calculations at the X-ray wavelength of 0.1033 nm (12.0 keV), for non-textured crystals exhibiting no extinction effects. At this wavelength, the 2θ range of the SRXRD detector (25° to 55°) contained three ferrite peaks: the bcc (110), bcc(200), and bcc(211), and three austenite peaks: the fcc(111), fcc(200) and fcc(220).

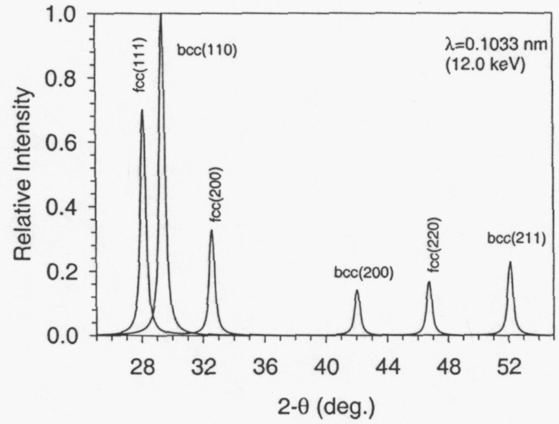

Figure 3: Calculated powder diffraction pattern for bcc-Fe and fcc-Fe at room temperature in the 2θ window of the SRXRD experiments.

An example of an SRXRD diffraction pattern taken from an HAZ location during welding where all six of the possible peaks are present is shown in Fig. 4. In this diffraction pattern, the fcc(111) and bcc(110) peaks are the most prominent features, with relative intensities close to those of the calculated powder diffraction pattern. However, this is not always the case because texture [21] in the weld HAZ can alter the relative intensities of the SRXRD diffraction patterns [12-15], particularly in the coarse grained region of the weld.

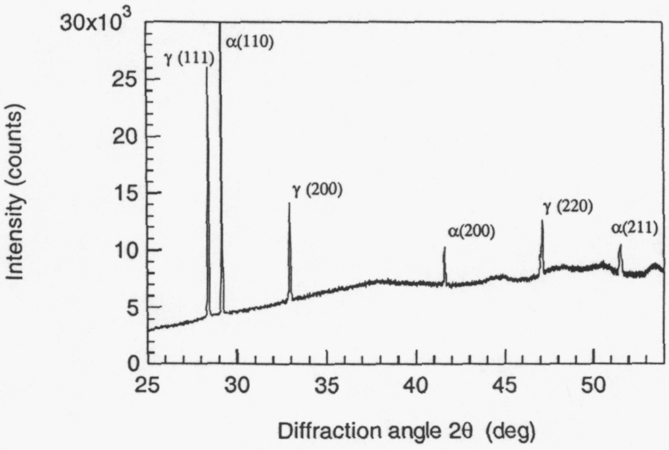

Figure 4: SRXRD pattern taken during welding at a location (x=-1, y=5.75 mm) where α-Fe and γ-Fe coexist.

Individual diffraction patterns were taken at discrete locations during each weld as the HAZ traversed beneath the stationary X-ray beam. Figure 5 shows a typical set of SRXRD diffraction patterns for one given weld. To gather this data, the beam was initially located in the liquid weld pool at a position 1 mm ahead of the electrode (x=-1.0) and 2 mm to the side of the electrode (y=2.0). The coordinate system used to represent the location of the x-ray beam with respect to the weld is shown in the schematic drawing that is inset in Fig. 5. This starting position placed the beam initially in the liquid weld pool, which yielded no Bragg peaks (characteristic of the liquid state) during the first 6 frames of this sequence. As the weld jogged to new positions, the X-ray beam passed through the liquid and reached the liquid/solid interface at frame number 7 where the first diffraction peaks were observed. From this point on, Bragg peaks appeared at all HAZ locations, showing the presence of the δ-Fe, γ-Fe and α-Fe phases. These phases change in relative proportions across the HAZ, indicating the phase transformations that are occurring during welding.

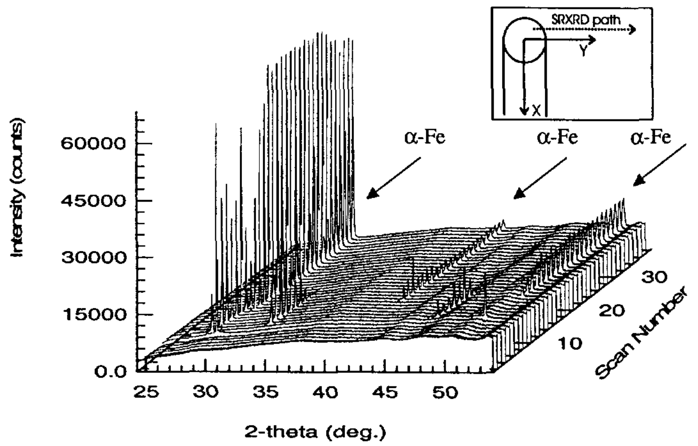

Figure 5: A typical complete SRXRD scan showing 37 diffraction patterns taken across the weld HAZ. Each successive diffraction pattern was taken at 0.25 mm steps along the y direction away from the weld centerline.

As the beam passed into the HAZ, the first two frames (7,8) contained δ-Fe peaks, and in both cases the δ-Fe coexisted with a small amount of γ-Fe. In the next 5 frames (9-13) only the γ-Fe diffraction peaks were observed, showing that this portion of the HAZ had been completely austenitized by the weld thermal cycle. In the next 6 frames (14-19) both γ-Fe and α-Fe diffraction peaks were observed, indicating the region of the HAZ where the partial transformation of α-Fe to γ-Fe had occurred. The remaining 17 frames (20-37) contained diffraction patterns only from α-Fe that was undergoing annealing and/or recrystallization. The maximum width of this HAZ is 3.25 mm as determined from the furthest SRXRD observation of the fcc phase from the fusion line. This width corresponds very well with the metallographic observations on the top surface of the weld, which showed that the outside edge of the partially transformed region of the HAZ extended 3.0 mm from the fusion line.

Spatially Resolved X-Ray Diffraction Map. The sequential x-ray diffraction line scans made perpendicular to the weld centerline, such as those presented in Fig. 5, were analyzed to determine the spatial distribution of the different phases. Each scan covered a distance of approximately 10 mm to span the width of the HAZ and contained 37 SRXRD patterns. A total of 21 individual line scans were made with the first scan at a location 6 mm ahead of the weld and the last scan at a location 17 mm behind the weld.

Figure 6 shows the completed phase map and the distribution of the α-Fe, γ-Fe, δ-Fe, and liquid phases in the HAZ. The coexistence of γ-Fe with α-Fe, or γ-Fe with δ-Fe, was identified at numerous SRXRD locations as evidenced by simultaneous recording of the fcc and bcc diffraction patterns. These regions indicate either a phase is in the process of transforming or that two phases are coexisting in a two-phase region of the HAZ.

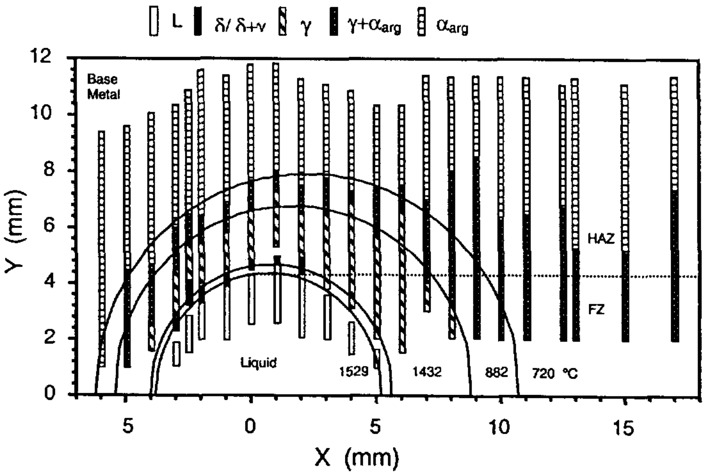

Figure 6: SRXRD map showing the locations of the α-Fe, γ-Fe, δ-Fe and liquid phases present in the AISI 1005 steel fusion weld at 1.9 kW. Regions where two phases co-existed are indicated with different shadings. The horizontal dotted line, y=4.4 mm, marks the average experimental fusion line of the weld.

Superimposed on Fig. 6 are four different weld isothermal boundaries calculated using an analytical heat flow model described in the Appendix. The calculated isotherm at 1529°C represents the liquid weld pool boundary, which extends 4.4 mm from the weld centerline, and was made to equal to the actual weld pool width by adjusting the heat source distribution parameter as discussed in [22]. The γ/(γ+δ) boundary is represented by the 1432°C isotherm, the γ/(γ+α) boundary is represented by the 882°C isotherm, and the $Fe_3C/(\alpha+\gamma)$ eutectoid is represented by the 720°C isotherm. These calculated boundaries represent the locations where phase transformations would occur under equilibrium conditions. However, since the kinetics of the phase transformations require a finite time to take place, the location where the phase transformation is finally completed is displaced behind the calculated isotherms. Thus, the calculated isotherms represent the point where the phase transformations *can* begin to occur; the locations where the transformations are complete can be determined by SRXRD measurements. The difference between the calculated isotherms (start locations) and the SRXRD completion locations is related to the kinetics of a given phase transformation.

HAZ Phase Transformation Regions on Heating. The α_{arg} phase region occurs where α-Fe was observed at temperatures too low for transformation to γ-Fe, but was undergoing annealing, recrystallization and/or grain growth. This region extends from the A1 isotherm out to the base metal, and is characterized by SRXRD patterns that show only the bcc diffraction peaks, as indicated by the regions shaded with horizontal stripes. In this region, the diffraction patterns gradually evolve from those of the base metal to those of the annealed and recrystallized microstructure.

These diffraction peaks are broad due to a combination cold work [21] resulting from surface machining of the steel bar, and from geometric effects from diffraction taking place over a finite distance on the curved surface of the sample bar [14]. During the heating cycle of the weld, α-Fe first begins to anneal, which has the effect of creating larger and more perfect diffraction domains than those of the base metal. This causes the diffraction peaks to reduce in width [14,21].

As α-Fe experiences more thermal exposure and higher welding temperatures, the α-Fe grains begin to recrystallize and yield very narrow diffraction. The recrystallized ferrite grains are small and nearly strain free, yielding very narrow diffraction peaks. These fine ferrite grains diffract to slightly different locations on the position sensitive x-ray detector, resulting in a tight grouping of individual spikes. These effects are similar to recrystallization observed in titanium welds using SRXRD [12,13] and the nature of the spikes in the resultant Bragg peaks is described in more detail elsewhere [14].

The α_{arg} + γ-Fe two-phase region is the next region closer to the weld fusion zone, where additional time and the higher temperature have caused α-Fe to partially transform to γ-Fe. This region, shown by the shaded dots, is moderately large because it exists over a 162°C temperature range between the A1 and A3 temperatures as illustrated in Fig. 1. In the α_{arg} + γ-Fe two-phase region of the weld, α-Fe and γ-Fe coexist in different volume fractions with the amount of γ-Fe increasing as the γ/(γ+α) boundary is approached. Behind the weld, the region(s) of the HAZ that transformed partially or completely to γ-Fe during weld heating, transforms back to α-Fe during weld cooling and leaves some residual γ-Fe in the miscrostructure.

The single-phase γ-Fe region is the next region closer to the weld fusion zone, where the time/temperature cycle has been sufficient to completely transform α-Fe to γ-Fe. The single-phase γ-Fe exists over a 550°C temperature range between the A_C3 and A_C4 temperatures as illustrated in Fig. 1. This wide temperature range results in an HAZ region for the γ-Fe phase which can extend more than 1.5 mm in width at its maximum point as indicated by the calculated isotherms. The regions shaded on the diagonal, show where SRXRD observed the single phase γ-Fe region, and indicate that this region first appears at a location about 4 mm ahead of the welding electrode. As the steel continues to be heated while passing beneath the arc, the γ-Fe region widens to about 1.5 mm past the fusion line as the transformation from α-Fe to γ-Fe occurs at locations farther from the fusion line.

The δ-Fe region is the closest region to the weld fusion zone, and the SRXRD measurements where the δ-Fe phase was observed are highlighted as the solid black regions. The δ-Fe phase was observed only within 0.5 mm of the liquid weld pool, and primarily on the leading edge of the weld pool. The experimental observations of δ-Fe on the leading edge of the weld pool are significant in that the presence of δ-Fe at the liquid/solid interface provides an epitaxial template for the liquid-to-solid transformation (solidification) to δ-Fe. In the HAZ, the δ-Fe that forms on heating transforms completely to γ-Fe just past the location where the weld pool is at its maximum width.

HAZ Phase Transformation Regions on Cooling. There are two different phase transformations that occur in the HAZ during cooling. The first is the δ-Fe to γ-Fe transformation at high temperature. The SRXRD measurements show that this transformation does indeed take place close to the weld pool and goes to completion over a short distance. No δ-Fe is observed beyond 2 mm behind the weld pool as indicated in Fig. 6. The second transformation is the γ-Fe to α_{bt}-Fe transformation, which occurs further away from the weld pool where the HAZ has cooled below the A_R3 temperature (882°C). This transformation is largely responsible for the microstructures that are present at room temperature since no other transformations occur after the back-transformed ferrite (α_{bt}-Fe) is formed.

The γ-Fe that transforms to α_{bt}-Fe may have three different origins within the HAZ: 1) γ-Fe that transformed from δ-Fe, 2) single-phase γ-Fe that completely transformed from α-Fe in the HAZ, or 3) γ-Fe that partially transformed from α-Fe coexisted with the remaining α-Fe in the HAZ. The α_{bt}-Fe that forms from these different phase regions of the HAZ (partially transformed region, fully austenitic region, delta ferrite region) create different microstructures after the weld has cooled to room temperature. These microstructures correspond to the coarse grained, fine-grained and partially transformed regions of the HAZ. These differences are the result of different nucleation and growth conditions for the γ-Fe to α_{bt}-Fe transformation.

The back transformed portion of the HAZ contains α_{bt}-Fe + γ-Fe, where γ-Fe was observed coexisting with α_{bt}-Fe. This region of the weld begins slightly behind the A_R3 isotherm (882°C), where the α_{bt}-Fe first nucleates and/or grows from γ-Fe. As the transformation to α_{bt}-Fe continues, the phase fraction of α_{bt}-Fe increases to the point where only small γ-Fe peaks are seen coexisting with the α_{bt}-Fe peaks. This latter region, where residual austenite (γ_r-Fe) remains in small quantities, is shown in Fig. 6 as the dotted region behind the weld. The γ_r-Fe region begins slightly behind the A_R1 isotherm (770°C) and remains to distances as far as 17 mm behind the weld, which is as far back as the SRXRD experiments were performed.

Conclusions

1. SRXRD was successfully used to map the phases occurring in the HAZ of gas tungsten arc welds in AISI 1005 steel. These measurements constitute the first *in-situ* and direct experimental investigations of phase transformations in steel welds, and the information contained within the HAZ phase map can be used to calculate phase transformation rates under true *non-isothermal* welding conditions.
2. Five principal microstructural regions were observed with SRXRD in the HAZ : (1) α-ferrite which is undergoing annealing, recrystallization and/or grain growth at subcritical temperatures, (2) partially transformed α-ferrite coexisting with γ-austenite at intercritical temperatures, (3) single phase γ-austenite at austenitizing temperatures, (4) δ-ferrite at temperatures near the liquidus temperature, and (5) back transformed α-ferrite co-existing with residual austenite at subcritical temperatures behind the weld.
3. The high temperature δ ferrite phase was observed at locations primarily within 0.5 mm of the liquid weld pool. The δ-Fe phase was observed to back transform quickly and completely to γ-Fe just past the location where the weld pool was at its maximum width. The presence of δ-Fe adjacent to the liquid weld pool provides the opportunity for epitaxial growth of the bcc phase from the liquid weld pool during solidification.

Acknowledgments

This work was performed under the auspices of the U. S. Department of Energy, Lawrence Livermore National Laboratory, under Contract No. W-7405-ENG-48. T. R. thanks the Alexander von Humboldt Foundation for a Feodor Lynen research fellowship. The synchrotron experiments were carried out at SSRL supported by DOE, the Division of Chemical Science. The authors would like to express their gratitude to Dr. Suresh Babu for assisting with the data analysis, Mr. A. T. Teruya of LLNL for writing the LabView software to control the welding experiments, and Mr. B. Kershaw of LLNL for performing optical metallography.

References

1. Ø. Grong, *Metallurgical Modelling of Welding*, The Institute of Materials, London, Chapter 1, (1994)
2. K. Easterling, *Introduction to the Physical Metallurgy of Welding*, Butterworths and Co., Chapter 3, (1983)
3. M. F. Ashby and K. E. Easterling, "A First Report on Diagrams for Grain Growth in Welds," *Acta Metall.*, V30, p. 1969, (1982)
4. J. C. Ion, K. E. Easterling, and M. F. Ashby, "A Second Report on Diagrams of Microstructure and Hardness for HAZ in Welds," *Acta Metall.*, V32, p. 1949, (1984)
5. M. Frewin, D. Dunne, and A. Scott, " Structural evolution of pulsed Nd-YAG laser welds of AISI 1006 steel," *Science and Technology of Welding and Joining*, V3(3), 9. 145, (1998)
6. M. F. Ashby and K. E. Easterling, "The Transformation Hardening of Steel Surfaces by Laser Beams—I. Hypo-Eutectoid Steels," *Acta Metall.*, V32, p. 1935, (1984)
7. Z. Yang and T. DebRoy, " Weld metal microstructure prediction from fundamentals of transport phenomena and phase transformation theory," *Science and Technology of Welding and Joining*, Vol 2(2), p. 1, (1997)
8. K. Mundra, T. DebRoy, S. S. Babu and S. A. David, " Weld Metal Microstructure Calculations from Fundamentals of Transport Phenomena in the Arc Welding of Low-Alloy Steels," *Welding Journal*, 76(4), p. 163-s, (1997)
9. Z. Yang and T. DebRoy, " Modeling Macro- and Microstructures of Gas-Metal-Arc Welded HSLA-A-100 Steel," *Metall. Mater. Trans. B, 30B,* pp. 483-493, (1999)
10. Z. Yang, J. W. Elmer, Joe Wong, and T. DebRoy, "Evolution of Titanium Arc Weldment Macro- and Microstructures – Modeling and Real Time Mapping of Phases," *Welding Journal*, 79(4), p. 97s-112s, (2000)
11. V. Karpenko, J.H. Kinney, S. Kulkarni, K. Neufeld, C. Poppe, K.G. Tirsell, Joe Wong, J. Cerino, T. Troxel, J. Yang, E. Hoyer, M. Green, D. Humpries, S. Marks, and D. Plate: *Rev. Sci. Instrum.*, 60, p.1451, (1989)
12. J. W. Elmer, Joe Wong, M. Fröba, P. A. Waide and E. M. Larson, "Analysis of Heat Affected Zone Phase Transformations Using In-Situ Spatially Resolved X-Ray Diffraction With Synchrotron Radiation," *Metall. Mater. Trans. A,* 27A(3), p. 775, (1996)
13. J. W. Elmer, Joe Wong and Thorsten Ressler, " Spatially Resolved X-Ray Diffraction Phase Mapping and $\alpha \rightarrow \beta \rightarrow \alpha$ Transformation Kinetics in the HAZ of Commercially Pure Titanium Arc Welds," *Metall. Mater. Trans. A*, 29A(11), p. 2761, (1998)
14. Thorsten Ressler, Joe Wong and J. W. Elmer, " Investigation of Real-Time Microstructure Evolution in Steep Thermal Gradients using Spatially Resolved X-ray Diffraction: A Case Study for Ti Fusion Welds," *J. Phys. Chem. B*, 102(52), p. 10724, (1998)
15. Joe Wong, M. Fröba, J. W. Elmer, and P. A. Waide "In-Situ Phase Mapping and Transformation Study in Fusion Welds," *J. Mat. Sc.*, 32, p. 1493, (1997)
16. R. W. K. Honeycomb, *Steels- Microstructure and Properties*, American Society of Metals, (1982)
17. B. Sundman, B. Jansson and J. Andersson: Calphad-Computer Coupling of Phase Diagrams and Thermochemistry, V 9(2), p.153, (1985)
18. Calculations performed by Dr. Suresh Babu of Oak Ridge National Laboratory, March, (2000)
19. *PowderCell, v. 1.0,* W. Kraus and G. Nolze, Federal Institute for Materials Research and Testing, Rudower Chaussee 5, 12489 Berlin, Germany. A free version may be obtained by request to gert.nolze@Bam.de.
20. Metals Handbook, Ninth Edition, Vol. 3, *ASM International*, (1979)
21. B. D. Cullity, *Elements of X-Ray Diffraction*, Addison Wesley, p. 263, (1956)
22. J. W. Elmer, Joe Wong and Thorsten Ressler : *Metall. and Mater. Trans. A*, 32A (5), pp. 1175-1187, (2001)